# Structure and grating efficiency of thin cells filled by a twist-bend nematic liquid crystal

M. Ali [1,2] E. Gorecka,[1] D. Pociecha [1] and N. Vaupotič [2,3,*]

[1]*Faculty of Chemistry, University of Warsaw, Zwirki i Wigury 101, 02-089 Warsaw, Poland*

[2]*Department of Physics, Faculty of Natural Sciences and Mathematics, University of Maribor, Koroška 160, 2000 Maribor, Slovenia*

[3]*Jožef Stefan Institute, Jamova 39, 1000 Ljubljana, Slovenia*

(Received 11 June 2020; accepted 31 August 2020; published 30 September 2020)

A twist-bend nematic ($N_{TB}$) liquid crystalline phase spontaneously forms modulated structures on a microscale level when confined in thin planar cells. Preliminary studies showed that these cells can be used as polarization gratings. Here we present a theoretical description of the formation of a two-dimensionally modulated structure. By considering the $N_{TB}$ phase as a pseudolayer medium, a threshold condition for the onset of a modulated structure is calculated for weak and strong boundary conditions in the case of initially bookshelf or pretilt alignment of pseudolayers. Based on the modeled structure we determine spatial variation of the optic axis and calculate properties of the transmitted diffracted light. Results of the beam propagation method (BPM) and transfer matrix method are compared and it is shown that a more complex BPM gives better agreement with experimental results, meaning that even in thin cells the diffraction of light inside the grating should not be neglected.

DOI: 10.1103/PhysRevE.102.032704

## I. INTRODUCTION

The self-assembly of deformed thin elastic layer systems has been given a lot of attention due to potential applications in soft robotics, photoactuators, and sensors, as well as fundamental research purposes [1]. Spontaneous deformations due to the bending, wrinkling, and twisting of layered structures are very well known in the lamellar phases of liquid crystals (LCs) such as the smectic-A phase (Sm-*A*), or in chiral nematics ($N^*$) with a helical twist deformation of the local average orientation of the long molecular axes, denoted by the nematic director $\vec{n}$ [2–4]. Under external stimuli and boundary constraints, layered LCs can relax the applied stress by curving around defects such as edge dislocations or arrange around line defects in focal conic domains and rotate periodically along a certain plane as first reported by Helfrich [5,6] and Hurault [7]. In their studies, the $N^*$ phase forms pseudolayers parallel to the confinement substrates, if the distance between the two substrates is much larger than the helical pitch of the director modulation. If an electric or magnetic field is applied normal to substrates, it causes the (pseudo-) layers to undulate periodically. In Refs. [5–7], a two-dimensional (2D) modulation was considered: (pseudo-) layers undulate in the direction along the surfaces; the amplitude of undulation depends on the distance of a specific layer from the surface. Subsequently, several studies related to two- (2D) and three-dimensional (3D) layer undulations in lamellar LCs induced by electric or magnetic field and also by dilative stress were reported [8–15]. Experimental observations of the 2D and 3D undulations in the $N^*$ phase confined in a planar cell [16,17] revealed that layers tend to undulate already on the substrates, so the assumption of strong anchoring of the surface layer assumed in the previous studies was released and finite surface anchoring was considered. By weakening the surface anchoring, the theoretically predicted amplitude of modulation became larger, which agreed with experimental observations. Under very high electric fields the pseudolayers adopted a sawtoothlike shape as predicted in Ref. [15].

Two decades ago, spontaneous chiral ordering was observed in the nematic phase made of achiral bent-core molecules [18–20]. A phase transition from the nematic to modulated nematic phase in achiral materials was observed [21] and the formation of the modulated structure was attributed to a twist-bend deformation of the nematic director [22], predicted theoretically [23,24] and by computer simulations [25]. Based on electro-optical studies of chiral domains, it was suggested that the director rotates on the cone with the helical pitch on the nanometer scale [26,27] and the structural characterization of this phase (named the twist-bend nematic, $N_{TB}$) showed that the helical pitch length is approximately 8−10 nm [28–30]. In fact, it seems that the structure is more complex than a simple helix; based on the results of the resonant soft x-ray scattering it was suggested that the structure consists of two shifted helices [31,32]. Since the identification of the $N_{TB}$ phase, various theoretical models were considered to predict the formation of a stable $N_{TB}$ phase, building the free energy (i) from the distortions of the pseudolayers and elastic deformations of the nematic director [33–35], also by including coupling with the polarization field [36]; (ii) from elastic deformations of the helical axis direction coupled to the magnitude of the cone angle [37]; (iii) from elastic deformations of the nematic director coupled to the spatial variation of the local polarization [38,39]; and (iv) by a more comprehensive Landau–de Gennes type free energy built from a tensorial order parameter of the nematic phase [40–43].

*Corresponding author: Natasa.Vaupotic@um.si

 

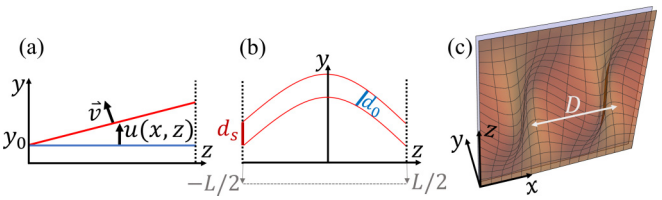


FIG. 1. (a) The pseudolayer that was initially at $y_0$ is displaced by $u(x, z)$; $\vec{v}$ is the pseudolayer normal. (b) By undulation, the pseudolayer thickness is reduced from $d_s$ to $d_0(T)$. (c) A 2D pseudolayer undulation with the period of modulation $D$ along the $x$ direction.

A confinement of the $N_{\mathrm{TB}}$ phase in planar cells with a uniform surface alignment yields a stripe texture and if the cell thickness is larger than 3 $\mu$m, stripes and focal conic domains coexist [21,26,27,44–49]. The periodicity of the stripe texture is always approximately twice the cell thickness [21,44–49]. The formation of a periodic structure is explained as follows [45,48,49]. Due to a short pitch of the heliconical modulation the $N_{\mathrm{TB}}$ phase behaves as a pseudolayered medium. The pitch of the heliconical modulation is strongly temperature dependent close to the $N$-$N_{\mathrm{TB}}$ phase transition; the modulation is formed at the phase transition and the pitch reduces when temperature is lowered. However, close to the surface, molecular positions are anchored by the surface forces, so the pitch close to the surface does not change. As a result, pseudolayers start to undulate in two directions: parallel to the surfaces (formation of a horizontal chevron) and perpendicular to the surfaces (formation of a vertical chevron) [Fig. 1(c)]. This leads to a spatial variation of the optic axis direction and, in turn, to the appearance of a stripe pattern in optical textures observed under a polarizing microscope. Due to a spatial variation of the optic axis direction, the stripe pattern acts as a grating, which diffracts light and affects its polarization properties. The polarization state of the zeroth order of the diffracted light depends on the retardation experienced by the incident beam when propagating through the material. For the first-order diffraction peaks the left circularly polarized (LCP) incident light transforms into right circularly polarized (RCP) light and horizontally linearly polarized (HLP) incident light transforms into vertically linearly polarized (VLP) light. For the second-order diffraction peaks, linearly polarized light transforms into elliptically polarized light, while LCP light transforms into almost diagonally linearly polarized (DLP) light and vice versa [48,49].

Preliminary studies of the optical properties of the $N_{\mathrm{TB}}$ grating have shown that the diffraction pattern is asymmetric both in amplitudes of the diffracted peaks as well as in polarization of the second-order diffracted peaks. A one-dimensional two-variable model was constructed to qualitatively predict the properties of the diffracted light [48]. This model assumes ad hoc the pseudolayer normal variation inside the cell and fits the model parameters to qualitatively match the experimental behavior. The model neglects the fact that the gratings are thick (the cell thickness is a few wavelengths of light) and that the pseudolayer normal direction varies also along the direction of light propagation. In this paper, we focus on the theoretical description of the formation of a 2D pseudolayer undulation of the $N_{\mathrm{TB}}$ phase filled in thin cells with planar surface boundary conditions. The threshold condition for the pseudolayer undulations is calculated for weak and strong boundary conditions for the case of initial bookshelf or tilted alignment of pseudolayers. Then we use the transfer matrix method (TMM) [50] and beam propagation method (BPM) [51] to calculate optical transmission properties of modulated structures and compare the results with experimental measurements. We show that it is essential to use the BPM to obtain good qualitative prediction of the experimental results, which is expected because on the level of wavelength of light the grating is thick, so the diffraction inside the grating cannot be neglected.

## II. THEORETICAL MODEL

The short-pitch heliconical arrangement of molecules in the $N_{\mathrm{TB}}$ phase can be regarded as a pseudolayer structure. The compressibility of the helical pitch is comparable to the compressibility of the smectic layers with the layer thickness equal to the heliconical pitch [52] and the direction of the heliconical axis is equivalent to the direction of a smectic layer normal. We are interested in the pseudolayer structure formed when a $N_{\mathrm{TB}}$ material is filled into planar cells of cell thickness ($L$) of the order of micrometers. The cell is filled with a material in the nematic phase and then cooled below the $N$-$N_{\mathrm{TB}}$ phase transition temperature.

At first, we assume that at the $N$-$N_{\mathrm{TB}}$ phase transition the heliconical arrangement of molecules is formed parallel to cell surfaces; thus pseudolayers are oriented perpendicular to the surfaces. The pseudolayer geometry is shown in Fig. 1. Upon the formation of the $N_{\mathrm{TB}}$ phase, the layer normal ($\vec{v}$) is along the $y$ axis and the heliconical pitch (the pseudolayer thickness) is $d_s$. When temperature ($T$) decreases, the heliconical pitch $d_0(T)$ reduces. If we assume that layers are strongly anchored at the surface, the only way to reduce the layer thickness is by undulating the layers. The displacement of a distorted layer is represented by a scalar variable $u$ (the displacement field). If we assume 2D modulation, the position ($y$) of a distorted layer that was initially at $y_0$ is given by $y = y_0 + u(x, z)$. The period of modulation along the $x$ axis is $D$.

We shall describe the 2D pseudolayer structure of the $N_{\mathrm{TB}}$ phase in terms of the nematic director field $\vec{n}$ (by which we describe the direction of the heliconical axis) and a complex smectic order parameter $\Psi$, the gradient of which gives the direction of the layer normal $\vec{v} = \frac{\nabla\Psi}{|\nabla\Psi|}$. The director $\vec{n}$ is assumed to be the parallel to the layer normal ($\vec{n}||\vec{v}$).

When the temperature is lowered, the heliconical pitch reduces. The competition between the surface strain due to anchoring and bulk strain causes elastic deformations that drive the undulation of pseudolayers. The free energy ($F$) of the structure is given by a sum of the integrated bulk ($f$) and surface ($f_a$) free energy densities,

$$F = \int f dV + \int f_a dS, \tag{1}$$

where $V$ and $S$ denote the cell volume and surface, respectively.

The bulk free energy density is expressed as a sum of nematic ($f_n$) and smectic ($f_s$) free energy densities [53–55],

$$f = f_n + f_s, \tag{2}$$

where

$$f_n = \tfrac{1}{2}\,K_{11}(\nabla\cdot\vec{n})^2 + \tfrac{1}{2}\,K_{22}(\vec{n}\cdot\nabla\times\vec{n})^2 + \tfrac{1}{2}K_{33}(\vec{n}\times\nabla\times\vec{n})^2, \tag{3}$$

with $K_{11}$, $K_{22}$, and $K_{33}$ being the elastic constants related to splay, twist, and bend deformations of the direction of the heliconical axis, respectively, and

$$f_s = C_\parallel|\vec{n}\cdot\nabla\Psi - i\,q_0(T)\Psi|^2 + C_\perp|\vec{n}\times\nabla\Psi|^2, \tag{4}$$

with $C_\parallel$ and $C_\perp$ describing the cost of compression of the layers and the cost of tilting the director $\hat{n}$ from the layer normal, respectively. The temperature dependence of the undulated layer of thickness $d_0(T)$ is described by $q_0(T) = 2\pi/d_0(T)$. By taking $\vec{n}\parallel\vec{v}$, the nematic contribution contains only the splay and bend elasticity, which describes the local variation of the heliconical axis, and the smectic part reduces to the compressibility of layers only, which accounts for the energy associated by the heliconical pitch not being equal to its equilibrium bulk value.

We assume that the direction of the heliconical pitch at the surface is strongly anchored, so the periodicity along the $y$ axis is defined by the heliconical pitch formed at the phase transition to the $N_{\mathrm{TB}}$ phase. The smectic order parameter for the distorted layer is thus expressed as

$$\Psi = \Psi_0\, e^{iq_s\,[y-u(x,z)]}, \tag{5}$$

where $\Psi_0$ is the amplitude and $q_s = 2\pi/d_s$ denotes the "frozen-in" periodicity of pseudolayers along the $y$ direction at the surfaces.

The position of layers at the surface does not change [$u(x,z)$ at both surfaces is zero]. The strength of the surface anchoring is defined in terms of the allowed tilt of the pseudolayers at the surface [16,17]. In the case of very strong anchoring, layers at the surface remain perpendicular to the surface [$\partial u(x,z)/\partial z = 0$]. In the case of very weak anchoring a general tilt is allowed. We shall study only the two limiting cases, and for the ansatz of the displacement field in the case of very strong anchoring we take

$$u(x,z) = u_0\left[\cos\left(\frac{2\pi}{L}z\right) + 1\right]\sin(q_x x), \tag{6}$$

where $u_0$ is the amplitude of modulation, and in the case of very weak anchoring,

$$u(x,z) = u_0\cos\left(\frac{\pi}{L}z\right)\sin(q_x x), \tag{7}$$

where $q_x = 2\pi/D$.

By using the above expressions for $u(x,z)$, we search for the threshold condition at which the modulated structure becomes stable with respect to the simple bookshelf geometry of pseudolayers. First, we transform $F$ into a dimensionless form by introducing the following dimensionless parameters:

$$\begin{aligned} \tilde{x} &= \frac{x}{L}, \quad \tilde{z} = \frac{z}{L}, \quad \tilde{y} = \frac{y}{L}, \\ \tilde{u}_0 &= \frac{u_0}{L}, \quad \tilde{K} = \frac{K_{33}}{K_{11}}, \\ \tilde{D} &= \frac{D}{L}, \quad \frac{C_\parallel q_s^2\Psi_0^2L^2}{K_{11}} = \frac{BL^2}{K_{11}} = \tilde{B}, \end{aligned} \tag{8}$$

where $B$ is the compressibility modulus.

The dimensionless free energy ($\tilde{F}$) per unit length along the $y$ direction is defined as

$$\tilde{F} = \frac{F}{K_{11}\tilde{D}} = \int_0^{\tilde{D}} d\tilde{x}\int_{-1/2}^{1/2}\tilde{f}\,d\tilde{z}, \tag{9}$$

where $\tilde{f}$ is a dimensionless free energy density.

### A. Strong boundary condition

The ansatz of the layer displacement under strong boundary conditions is given by Eq. (6). The dimensionless free energy up to the fourth order in $\tilde{u}_0$ is

$$\tilde{F} = \tilde{B}(-1 + q_{0s})^2 + A_2\tilde{u}_0^2 + A_4\tilde{u}_0^4, \tag{10}$$

where

$$q_{0s} = \frac{q_0(T)}{q_s} = \frac{d_s}{d_0(T)} \approx 1 + \frac{d_s - d_0(T)}{d_s} \tag{11}$$

is the ratio between the helical pitch at temperature $T$ and at the phase transition temperature, and parameters $A_2$ and $A_4$ are

$$A_2 = \frac{\pi^2}{\tilde{D}^4}[-\tilde{B}(-1+q_{0s})\tilde{D}^2(3+\tilde{D}^2) + 2\pi^2(3+2\tilde{D}^2+\tilde{D}^4)], \tag{12}$$

and

$$A_4 = \frac{\pi^4\tilde{B}q_{0s}}{16\tilde{D}^4}(105 + 10\tilde{D}^2 + 9\tilde{D}^4), \tag{13}$$

where we took into account that $\tilde{B} \gg 1$ ($\tilde{B}\sim 10^5$ if $K_{11}\sim 10^{-11}$ N, $L\sim 10^{-6}$ m, and $B\sim 10^6$ Pa) and $\tilde{K}\leqslant 1$.

The modulated structure is stable with respect to the bookshelf geometry when its energy becomes lower than the energy of the bookshelf structure with contracted layers. This happens at $q_{0s}$ larger than the threshold value $q_{0s}^{(th)}$.

The amplitude of the undulation $\tilde{u}_0$ and period of modulation $\tilde{D}$ are calculated by minimizing the free energy [Eq. (10)] over $\tilde{u}_0$ and $\tilde{D}$. We find $\tilde{u}_0 = \sqrt{-A_2/(2A_4)}$, which in the limit of $\tilde{B}\gg 1$ reduces to

$$\tilde{u}_0 = \frac{2\sqrt{2}\tilde{D}}{\pi}\sqrt{\frac{3+\tilde{D}^2}{105+10\tilde{D}^2+9\tilde{D}^4}}\sqrt{1-\frac{1}{q_{0s}}}\,. \tag{14}$$

For $\tilde{D}$ we obtain the condition

$$2A_4\frac{\partial A_2}{\partial\tilde{D}} - A_2\frac{\partial A_4}{\partial\tilde{D}} = 0\,. \tag{15}$$

In the limit of $\tilde{B}\gg 1$ and far from the threshold this simplifies to

$$\tilde{D} = \sqrt{\frac{45}{11}} \approx 2. \tag{16}$$

We see that the period of modulation along the $x$ axis is temperature independent and approximately twice the cell thickness. By plugging this value into the expression for $\tilde{u}_0$, we obtain

$$\tilde{u}_0 = 0.28\sqrt{1 - \frac{1}{q_{0s}}}\,. \tag{17}$$

To obtain $\tilde{D}$ close to the threshold value, we start by calculating $\tilde{D}$ numerically at a given set of parameters $\tilde{B}$, $\tilde{K}$, and $q_{0s}$. Then we check if the structure at a given $q_{0s}$ and calculated $\tilde{D}$ is stable. This is done in the following way: We write the free energy [Eq. (10)] by considering the equilibrium expression for $\tilde{u}_0$ to find $F = \tilde{B}(-1 + q_{0s})^2 - A_2^2/(4A_4)$ and then find the second derivative of $F$ over $\tilde{D}$. The structure is stable as long as this value is positive. In this way we find that $\tilde{D}_{th} \approx 6$ at the threshold, but it reduces to approximately 2 already within a relative change of pseudolayer thickness of $10^{-3}$.

The threshold value of $q_{0s}$ is found to be inversely proportional to the compressibility modulus:

$$q_{0s}^{(th)} \approx 1 + \frac{12.0}{\tilde{B}}\,. \tag{18}$$

The second term in Eq. (18) is of the order of $10^{-4}$ or lower, so the modulation becomes stable already at very small changes of the helical pitch, which means very close to the $N$-$N_{\mathrm{TB}}$ phase transition.

### B. Weak boundary condition

The ansatz for the weak anchoring conditions is given by Eq. (7). By following the same procedure as in the case of strong anchoring, we first calculate the dimensionless free energy which, up to the fourth order in $\tilde{u}_0$, has the same shape as given in Eq. (10), but with

$$A_2 = \frac{\pi^2(4 + \tilde{D}^2)}{8\,\tilde{D}^4}[-2\tilde{B}(-1 + q_{0s})\tilde{D}^2 + \pi^2(4 + \tilde{D}^2)], \tag{19}$$

and assuming $\tilde{B} \gg 1$ and $\tilde{K} \leqslant 1$,

$$A_4 = \frac{\pi^4 \widetilde{B}\, q_{0s}}{256\,\tilde{D}^4}(144 + 8\tilde{D}^2 + 9\tilde{D}^4). \tag{20}$$

By following the same procedure as in the case of strong anchoring, we find the modulation period at $\tilde{B} \gg 1$,

$$\tilde{D} = 2\,, \tag{21}$$

and the amplitude of modulation being twice that found for the strong anchoring case,

$$\tilde{u}_0 = 0.57\sqrt{1 - \frac{1}{q_{0s}}}\,. \tag{22}$$

As in the case of strong anchoring, the modulation period increases very close to the threshold value $q_{0s}^{(th)}$, but in the case of weak anchoring it increases up to $\tilde{D}_{th} \approx 70$. The threshold is found to be

$$q_{0s}^{(th)} \approx 1 + \frac{10.5}{\tilde{B}}\,. \tag{23}$$

From Eqs. (18) and (23) we see that the threshold value of $q_{0s}^{(th)}$ is higher in the case of the strong boundary conditions and the amplitude of modulation is larger in the case of weak anchoring. Both results are expected.

### C. Pretilt of pseudolayers with strong and weak boundary conditions

So far, we assumed that pseudolayers formed at the phase transition to the $N_{\mathrm{TB}}$ phase are perpendicular to the surface planes. This means that the heliconical axis is along the surface, which means that molecules at the surface are tilted. If we assume that molecules at the surface lie in the surface plane, then the pseudolayer structure formed at the phase transition is, in fact, tilted with respect to the surface, the tilt being equal to the initial cone angle value. So, within the next approximation, we assume that some finite pretilt of pseudolayers freezes in at the phase transition and that these tilted layers start to undulate when temperature is further reduced. Again, we study both the weak and strong anchoring and for $u(x, z)$ we use Eqs. (6) and (7) by adding a term $\gamma z$, where $\gamma$ is the pretilt angle, assuming that the pretilt is small. Therefore, for strong anchoring we have

$$u(x, z) = \gamma z + u_0\left[\cos\left(\frac{2\pi}{L}z\right) + 1\right]\sin(q_x x), \tag{24}$$

and for weak anchoring,

$$u(x, z) = \gamma z + u_0 \cos\left(\frac{\pi}{L}z\right)\sin(q_x x)\,. \tag{25}$$

Even in the limiting cases the expressions for the equilibrium and threshold values now become too long and complicated to be reproduced here. Instead, we give results at a given set of parameters: a chosen set of values of $\tilde{B}$, $\tilde{K}$, $q_{0s}$, and $\gamma$. The values for the modulation amplitude and modulation period as a function of $q_{0s}$ at $\tilde{B} = 5 \times 10^5$ are given in Fig. 2 for weak and strong anchoring conditions. The threshold values are collected in Table I. The values are practically independent of the value of $\tilde{K}$, because it is of the order of 1 or lower and is thus much lower than $\tilde{B}$.

We see that close to the threshold the behavior is much different compared to the nontilted case: $\tilde{D}$ close to the threshold is lower than 2 and the variation of $\tilde{D}$ is significant within the region of up to 10% change in the pseudolayer thickness (which can be experimentally detected), as opposed to the nontilted case where $\tilde{D}$ is predicted to vary only within a region of 0.1% of change of pseudolayer thickness below the threshold value for the formation of the modulated structure.

## III. OPTICAL PROPERTIES

In this section, we study optical properties of the diffraction grating formed by the modulation of the pseudolayer structure discussed in the previous section. We consider the $N_{\mathrm{TB}}$ phase as an optically uniaxial material with the local optic axis along the pseudolayer normal $\vec{v}$. From Eq. (5) we calculate

$$\vec{v}(x, z) = \frac{\nabla\Psi}{|\nabla\Psi|} = \frac{\left(-\frac{\partial u}{\partial x}, 1, -\frac{\partial u}{\partial z}\right)}{\sqrt{1 + \left(\frac{\partial u}{\partial x}\right)^2 + \left(\frac{\partial u}{\partial z}\right)^2}}, \tag{26}$$

which can be expressed as

$$\vec{v}(x, z) = (\sin\alpha\cos\beta, \cos\alpha\cos\beta, \sin\beta), \tag{27}$$

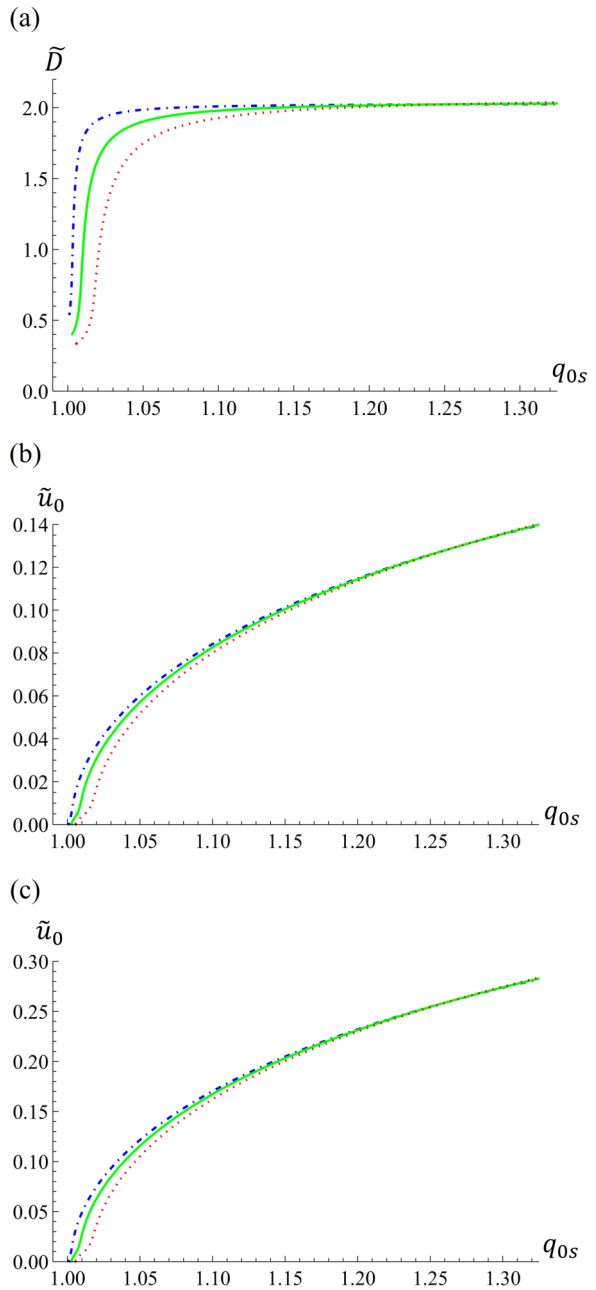


FIG. 2. Pretilt of pseudolayers. (a) The period of modulation $\tilde{D}$ is practically the same for weak and strong anchoring. Amplitude of modulation $\tilde{u}_0$ as a function of pretilt $\gamma$; the dot-dashed (blue), solid (green), and dotted (red) lines represent $\gamma = 0.04,\ 0.07,\ 0.1$, respectively: (b) strong and (c) weak anchoring. Parameter values: $\tilde{B} = 5 \times 10^5$, $\tilde{\mathrm{K}} = 1$.

where angles $\alpha$ and $\beta$ are defined in Fig. 3 and are both functions of $x$ and $z$. The angle $\pi/2 - \beta$ is the angle between the optic axis and the wave vector, while the angle $\alpha$ defines the projection of the optic axis to the $xy$ plane.

### A. Transfer matrix method

First, we calculate properties of the transmitted light by the transfer matrix method. With this method, we neglect the diffraction of light inside the cell. The part of the incident wave that enters the cell at position $x$ is assumed to obtain an additional phase due to the propagation through the material, which has a varying direction of the optic axis along the direction of light propagation ($z$ direction).

TABLE I. The ratio between the pseudolayer thicknesses at the threshold temperature and at the phase transition to the $N_{\mathrm{TB}}$ phase ($q_{0s}^{(th)}$), period of modulation at the threshold ($\tilde{D}_{th}$), in the case with and without the pretilt $\gamma$ at weak and strong anchoring. Parameter values: $\tilde{B} = 5 \times 10^5$; $\tilde{K} = 1$.

| Anchoring | $\gamma$ | $\tilde{D}_{th}$ | $q_{0s}^{(th)} - 1$ |
|---|---|---|---|
| Strong | 0 | 6.3 | $2.4 \times 10^{-5}$ |
| Strong | 0.04 | 0.54 | $1.1 \times 10^{-3}$ |
| Weak | 0 | 71 | $2.1 \times 10^{-5}$ |
| Weak | 0.04 | 0.58 | $1.05 \times 10^{-3}$ |

The numerical procedure goes as follows. The cell is divided into thin slices of thickness $\Delta z = L/n_z$, where $n_z$ is an integer. The position along the $z$ axis is defined by an integer $j$, $0 \leqslant j \leqslant n_z$, as $z_j = -L/2 + j\Delta z$. Within a slice, the direction of the optic axis along the $z$ direction is assumed to be constant. At the beginning of each slice the electric field is divided into the ordinary and extraordinary components and the phase difference between them upon the propagation through the slice is $\Delta\varphi = k_0 \Delta n \Delta z$, where $k_0 = 2\pi/\lambda$ is the wave number in vacuum, $\lambda$ is the wavelength of light, and the difference in indices of refraction between the extraordinary and ordinary waves ($\Delta n$) is

$$\Delta n = \sqrt{\left(\frac{\sin^2\beta}{n_o^2} + \frac{\cos^2\beta}{n_e^2}\right)^{-1}} - n_o, \tag{28}$$

where $n_o$ and $n_e$ are the ordinary and extraordinary index of refraction, respectively. By comparing Eqs. (26) and (27) we find

$$\cos^2\beta = \frac{1 + \left(\frac{\partial u}{\partial x}\right)^2}{1 + \left(\frac{\partial u}{\partial x}\right)^2 + \left(\frac{\partial u}{\partial z}\right)^2}, \tag{29}$$

and $\sin^2\beta = 1 - \cos^2\beta$. The birefringence $n_e - n_o$ is temperature dependent and it decreases on cooling of the $N_{\mathrm{TB}}$ phase.

The transfer matrix $M(x, z)$ for the slice at position $z$ connects the incident (at $z$) and exiting (at $z + \Delta z$) field components ($\psi_x$, $\psi_y$, only the slowly varying part is considered)

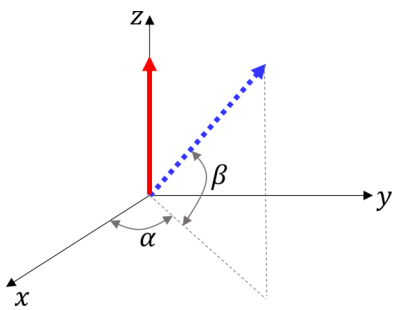


FIG. 3. Definition of angles $\alpha$ and $\beta$; solid (red) arrow along the $z$ axis and dotted (blue) arrow represent the wave vector direction and optic axis, respectively.

in the laboratory coordinate system,

$$\begin{pmatrix}\psi_x(x,z+\Delta z)\\ \psi_y(x,z+\Delta z)\end{pmatrix} = \underline{M}(x,z)\begin{pmatrix}\psi_x(x,z)\\ \psi_y(x,z)\end{pmatrix}, \tag{30}$$

where (see, for example, supplemental material to [48]):

$$\underline{M}(x,z) = \begin{pmatrix}M_{11} & M_{12}\\ M_{21} & M_{22}\end{pmatrix}, \tag{31}$$

with

$$\begin{aligned} M_{11} &= 1+\sin^2\alpha\,(e^{i\Delta\varphi}-1),\\ M_{12} &= M_{21} = -\sin\alpha\cos\alpha\,(e^{i\Delta\varphi}-1),\\ M_{22} &= 1+\cos^2\alpha\,(e^{i\Delta\varphi}-1). \end{aligned} \tag{32}$$

By comparing Eqs. (26) and (27) it is straightforward to obtain

$$\begin{aligned} \cos^2\alpha &= \left[1+\left(\frac{\partial u}{\partial x}\right)^2\right]^{-1},\\ \sin\alpha\cos\alpha &= -\frac{\partial u}{\partial x}\left[1+\left(\frac{\partial u}{\partial x}\right)^2\right]^{-1}. \end{aligned} \tag{33}$$

The field components $\psi_x(x, z = L/2)$ and $\psi_y(x, z = L/2)$ are obtained by a successive multiplication of matrices $M(x, z)$ at given positions $x$ and $z$ ranging from $-L/2$ to $L/2$. The field components at $z = -L/2$ are obtained by applying boundary conditions for the transverse electric and magnetic field at the air-liquid crystal interface. In the case of strong anchoring, the optic axis at the boundary lies in the $yz$ plane $\vec{v}(x, \pm L/2) = (0, 1, \gamma)/\sqrt{1+\gamma^2}$ and the field components inside the LC are related to the field components in air as (assuming that $\gamma \ll 1$)

$$\begin{pmatrix}\psi_x^{(\mathrm{LC})}\left(x,-\frac{L}{2}\right)\\ \psi_y^{(\mathrm{LC})}\left(x,-\frac{L}{2}\right)\end{pmatrix} = \begin{pmatrix}\psi_x^{(\mathrm{air,in})}\tau_o\\ \psi_y^{(\mathrm{air,in})}\tau_e\end{pmatrix}, \tag{34}$$

where the transmission coefficients are $\tau_o = 2/(1+n_o^2)$ and $\tau_e = 2/(1+n_e^2)$, and similarly at the interface at $z = L/2$, where

$$\begin{pmatrix}\psi_x^{(\mathrm{air,out})}\\ \psi_y^{(\mathrm{air,out})}\end{pmatrix} = \begin{pmatrix}\psi_x^{(\mathrm{LC})}\left(x,\frac{L}{2}\right)\tau_o\\ \psi_y^{(\mathrm{LC})}\left(x,\frac{L}{2}\right)\tau_e\end{pmatrix}, \tag{35}$$

but here the transmission coefficients are $\tau_o = 2/(1+n_o^{-2})$ and $\tau_e = 2/(1+n_e^{-2})$.

The components of the electric field of light propagating in the direction given by the $x$ component of the scattering vector $(q)$ are obtained by the Fourier transform:

$$\begin{pmatrix}\psi_x^{(q)}\\ \psi_y^{(q)}\end{pmatrix} = \left[\int_0^D \begin{pmatrix}\psi_x^{(\mathrm{air,out})}\\ \psi_y^{(\mathrm{air,out})}\end{pmatrix} e^{iqx}dx\right]\left(\sum_{j=0}^{N-1} e^{iqDj}\right), \tag{36}$$

where $N$ is the number of illuminated periods. The interference peaks are observed around $q = m2\pi/D$, with $m = 0, \pm1, \pm2\ldots$. The electric field components of the transmitted light are

$$\begin{pmatrix}E_x^{(q)}\\ E_y^{(q)}\end{pmatrix} = \begin{pmatrix}\left|\psi_x^{(q)}\right|\cos(\varphi_x-\omega t)\\ \left|\psi_y^{(q)}\right|\cos(\varphi_y-\omega t)\end{pmatrix}, \tag{37}$$

where we used $\psi_x^{(q)} = |\psi_x^{(q)}|\exp(i\varphi_x)$ and equivalently for the $y$ component, and the dependence on time $(t)$ was added; $\omega$ is the angular frequency of light.

### B. Beam propagation method

By the beam propagation method [51], we consider also the diffraction of light inside the grating. The propagation of light in an anisotropic medium is described by the wave equation,

$$\nabla\times[\nabla\times\vec{E}(x,z)] - k_0^2\underline{\varepsilon}(x,z)\cdot\vec{E}(x,z) = 0, \tag{38}$$

where $\underline{\varepsilon}(x, z)$ is a symmetric dielectric tensor of a uniaxial material,

$$\underline{\varepsilon} = \begin{bmatrix}\varepsilon_{11} & \varepsilon_{12} & \varepsilon_{13}\\ \varepsilon_{12} & \varepsilon_{22} & \varepsilon_{23}\\ \varepsilon_{13} & \varepsilon_{23} & \varepsilon_{33}\end{bmatrix}, \tag{39}$$

with the following elements in the laboratory system if the optic axis direction is given by $\vec{v}(x, z)$ [Eq. (26)]:

$$\begin{aligned} \varepsilon_{11} &= \varepsilon_\perp + \Delta\varepsilon(\sin^2\alpha\cos^2\beta),\\ \varepsilon_{22} &= \varepsilon_\perp + \Delta\varepsilon(\cos^2\alpha\cos^2\beta),\\ \varepsilon_{33} &= \varepsilon_\perp + \Delta\varepsilon(\sin^2\beta),\\ \varepsilon_{12} &= \Delta\varepsilon\sin\alpha\cos\alpha\cos^2\beta,\\ \varepsilon_{13} &= \Delta\varepsilon\sin\beta\sin\alpha\cos\beta,\\ \varepsilon_{23} &= \Delta\varepsilon\cos\alpha\cos\beta\sin\beta, \end{aligned} \tag{40}$$

where $\varepsilon_\perp = n_o^2$ and $\Delta\varepsilon = n_e^2 - n_o^2$.

By the slowly varying envelope approximation we separate the electric field components into a product of a slowly varying complex field and a rapidly varying phase along the $z$ direction:

$$\vec{E}(x,z) = \begin{pmatrix}\psi_x(x,z)\\ \psi_y(x,z)\\ \psi_z(x,z)\end{pmatrix}e^{ik_0n_oz}. \tag{41}$$

We plug Eqs. (40) and (41) into the wave equation (38), assume

$$\begin{aligned} \frac{\partial^2\psi_x}{\partial z^2} &\ll 2n_ok_0\frac{\partial\psi_x}{\partial z},\\ \frac{\partial^2\psi_y}{\partial z^2} &\ll 2n_ok_0\frac{\partial\psi_y}{\partial z} \end{aligned} \tag{42}$$

and obtain

$$\begin{aligned} 2ik_0n_o\frac{\partial\psi_x}{\partial z} &= k_0^2n_o^2\psi_x - k_0^2(\varepsilon_{11}\psi_x+\varepsilon_{12}\psi_y+\varepsilon_{13}\psi z)\\ &\quad + ik_0n_o\frac{\partial\psi_z}{\partial x} + \frac{\partial^2\psi_z}{\partial x\partial z}, \end{aligned} \tag{43}$$

$$2ik_0n_o\frac{\partial\psi_y}{\partial z} = k_0^2n_o^2\psi_y - k_0^2(\varepsilon_{12}\psi_x+\varepsilon_{22}\psi_y+\varepsilon_{23}\psi z) - \frac{\partial^2\psi_y}{\partial x^2}. \tag{44}$$

The longitudinal component of the electric field is calculated from Gauss's law:

$$\frac{\partial \psi_z}{\partial z} = -\frac{1}{\varepsilon_{33}}\left\{\frac{\partial(\varepsilon_{11}\psi_x)}{\partial x} + \frac{\partial(\varepsilon_{12}\psi_y)}{\partial x} + \frac{\partial(\varepsilon_{13}\psi_z)}{\partial x} + \frac{\partial(\varepsilon_{13}\psi_x)}{\partial z} + \frac{\partial(\varepsilon_{23}\psi_y)}{\partial z} + ik_0 n_0(\varepsilon_{13}\psi_x + \varepsilon_{23}\psi_y + \varepsilon_{33}\psi_z) + \psi_z\frac{\partial \varepsilon_{33}}{\partial z}\right\}. \quad (45)$$

To solve Eqs. (43)–(45), the explicit finite difference technique is adopted [51]. Again, along the $z$ direction, the cell is sliced into parts of thickness $\Delta z = L/n_z$, $n_z$ being an integer number, and along the $x$ direction one period of modulation is sliced into parts of width $\Delta x = D/n_x$, $n_x$ being an integer number. The position $(x, z)$ is given by $(x_l, z_j)$, where $x_l = l\Delta x$ and $z_j = -\frac{L}{2} + j\Delta z$. A periodic boundary condition is applied at $x = 0$ and $x = D$: $x_{-1} = x_{n_x-1}$ and $x_{n_x+1} = x_1$.

The numerical method is stable if steps along the $x$ and $z$ directions are chosen such that the following condition is fulfilled [51]:

$$\Delta z \leqslant \frac{(\Delta x)^2 n_0 \pi}{\lambda}. \quad (46)$$

The initial values of the field components $\psi_x(x, -L/2)$, $\psi_y(x, -L/2)$ are obtained as explained in the previous subsection; see Eq. (34). In the case of strong anchoring and small $\gamma$, the transverse component is approximately zero: $\psi_z(x, -L/2) \approx 0$.

At $z = L/2$, the $x$ and $y$ components are calculated as given by Eq. (35). The $z$ component is obtained by the conservation of the normal component of the displacement field, so

$$\psi_z^{(\mathrm{air})} = \varepsilon_{33}\psi_z^{(\mathrm{LC})}\left(x, \frac{L}{2}\right), \quad (47)$$

where the reflected field at the upper boundary was assumed to be much lower than the incident field $\psi_z^{(\mathrm{LC})}(x, \frac{L}{2})$. The Fourier components of the electric field in the transmitted light $(E_x^{(q)}, E_y^{(q)})$ are calculated from Eqs. (36) and (37).

### C. Polarization properties of the diffracted light

Polarization properties of the diffracted light are given by the azimuth angle $\psi$ and ellipticity $e$ or/and as a point on the Poincaré sphere (see Fig. 4).

The intensity and polarization properties of the central and the first- and second-order diffraction peaks are calculated by TMM and BPM and the results are compared to experimental values. Because the experimental diffraction pattern is asymmetric, we use theoretical results for the pretilt case. The pretilt leads to the asymmetry in birefringence, because the tilt angle $\beta$ [Eq. (29)] becomes asymmetric, while the tilt angle $\alpha$ [Eq. (33)] remains symmetric. The asymmetry in the phase lag between the ordinary and extraordinary waves results in the asymmetry of polarization properties of the diffracted light. For the central and the first-order peaks theoretical predictions are in line with experimental observations: polarization of the first-order diffracted wave remains linear for the linearly polarized incident light, but changes the direction, so VLP is transformed to HLP and vice versa, while DLP does not change and LCP transforms into RCP. For the central peak, polarization of light depends on the temperature and thickness of the cell, the first defining the birefringence, which together with $L$ defines the net phase difference between the ordinary and extraordinary wave upon traversing the cell. The internal structure of the cell has the biggest effect on the polarization properties of the second-order diffracted peaks, which we study in detail below.

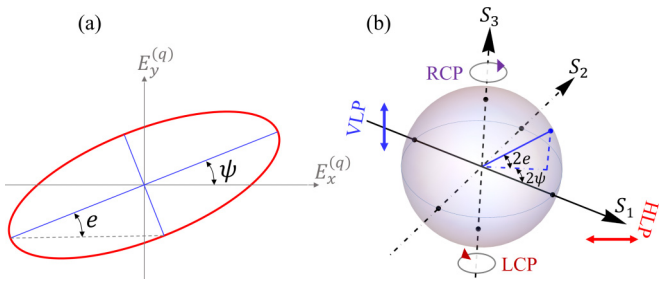


FIG. 4. (a) Polarization of light is defined by the azimuth angle $\psi$ and ellipticity $e$. (b) Polarization can be presented on the Poincaré sphere by a point the coordinates of which are given by the normalized values of the Stokes parameters $(s_1,\ s_2,\ s_3)$, where $s_1 = \cos(2\psi)\cos(2e)$ (solid arrow), $s_2 = \sin(2\psi)\cos(2e)$ (dash-dotted arrow), and $s_3 = \sin(2e)$ (dashed arrow).

From the TMM, the second-order diffracted peaks for the linearly polarized incident light remain linearly polarized: HLP remains HLP and VLP remains VLP, but, experimentally, a very small ellipticity is observed. This polarization change can be obtained only if BPM is used and strong anchoring is assumed. Experimentally, the internal structure of the cell has the greatest effect on the change of polarization of the circularly polarized incident light, so LCP incident light will be considered in further discussion.

In calculation, we focus first on CB7CB material. We used $\tilde{B} = 5 \times 10^5$, $\tilde{K} = 1$, and $\gamma = 0.04$ and assumed strong anchoring, due to the reason described in the previous paragraph. The value of $\gamma$ was chosen such that the best qualitative fit between the theoretical prediction and experimental results was obtained. It was assumed that the amplitudes $\alpha_0$ and $\beta_0$ of angles $\alpha$ and $\beta$ far from the phase transition temperature are approximately equal to the tilt of molecules with respect to the heliconical axis. In the case of strong anchoring with pretilt we use Eq. (24) for $u(x, z)$ and plug it into Eq. (33) to find

$$\tan\alpha_0 = 4\pi\tilde{u}_0/\tilde{D}, \quad (48)$$

and then into Eq. (29) to obtain

$$\tan\beta_0 = 2\pi\tilde{u}_0 - \gamma. \quad (49)$$

Experimentally, $\alpha_0 \approx 37^\circ$ at the temperature approximately 40 K below the phase transition temperature and by taking $\tilde{D} = 2$, we find $\tilde{u}_0 \approx 0.12$. From Fig. 2(b) we find that this value corresponds to $q_{0s} \approx 1.22$. In such a way we estimate the maximum value of $q_{0s}$ that needs to be considered. Next, the values of $q_{0s}$ are matched to the corresponding temperatures (Fig. 5) in the following way: At a specific value of $q_{0s}$, we first find $\tilde{D}$ and $\tilde{u}_0$ (Fig. 2). Then we calculate amplitudes of angles $\alpha$ and $\beta$ from Eqs. (48) and (49). These angles approximately match the cone angles calculated from

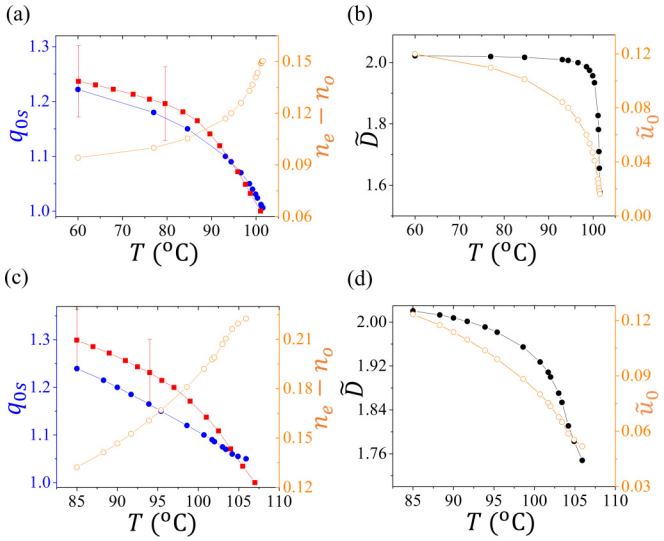


FIG. 5. Temperature ($T$) dependence of birefringence $n_e - n_o$ (experimentally measured), $q_{0s}$, $\tilde{D}$, and $\tilde{u}_0$, the latter two calculated in the case of strong anchoring with pretilt at the values of $q_{0s}$ denoted by blue filled circles in the left graph. (a), (b) CB7CB with $\gamma = 0.04$; (c), (d) CB6OCB with $\gamma = 0.1$. Parameter values: $\tilde{B} = 5 \times 10^5$, $\tilde{K} = 1$. In (a), (c) we give also experimentally measured ratio $q_{0s}^{(\mathrm{expt})} = q/q_{\min}$ (red filled squares), obtained by the resonant soft x-ray scattering [31,58], where $q_{\min} = 2\pi/d_s$ and $d_s$ is the pitch measured at the phase transition temperature. The error bars on two points are added to give the impression of the experimental error (approximately 10%).

the measured birefringence $n_e - n_o$ [48,56] at a certain temperature, and this temperature is then assigned to a chosen $q_{0s}$. The temperature dependences of the experimentally measured birefringence and theoretically calculated $q_{0s}$, $\tilde{D}$, and $\tilde{u}_0$ are given in Figs. 5(a) and 5(a). The procedure was repeated for CB6OCB [57] and the temperature dependencies of the above parameters are given in Figs. 5(c) and 5(d).

Figure 6 shows polarization of the second-order diffracted peaks $\pm 2q_0$, where $q_0 = 2\pi/D$. Experimental values, results of the preliminary model [48,49], and theoretically calculated values by TMM and BPM are given. The cell thickness was $L = 1.6\ \mu$m (CB7CB) and $L = 1.5\ \mu$m (CB6OCB), $n_x = 40$, and $n_z = 10\,000$. The large number $n_z$ is not defined by the condition in Eq. (46), but rather by the requirement that the intensity of light at $z = \pm L/2$ is the same (because we do not consider reflection and absorption inside the cell). We see that there is a difference between the results obtained by TMM and BPM, in particular the positions of the $+2q_0$ and $-2q_0$ peaks on the Poincaré sphere are exchanged in TMM compared to experimental results. The asymmetry is larger when BPM is used and it increases if the pretilt $\gamma$ increases. Theoretical figures lack the part of uniform ellipticity far from the phase transition, because the harmonic approximation that we used is valid only close to the phase transition temperature. Nevertheless, we see that the approximation gives good results in the whole temperature region over which the birefringence changes significantly. We see that by modeling the structure inside the cell, we obtain a good prediction of the qualitative behavior of the polarization properties of the second-order

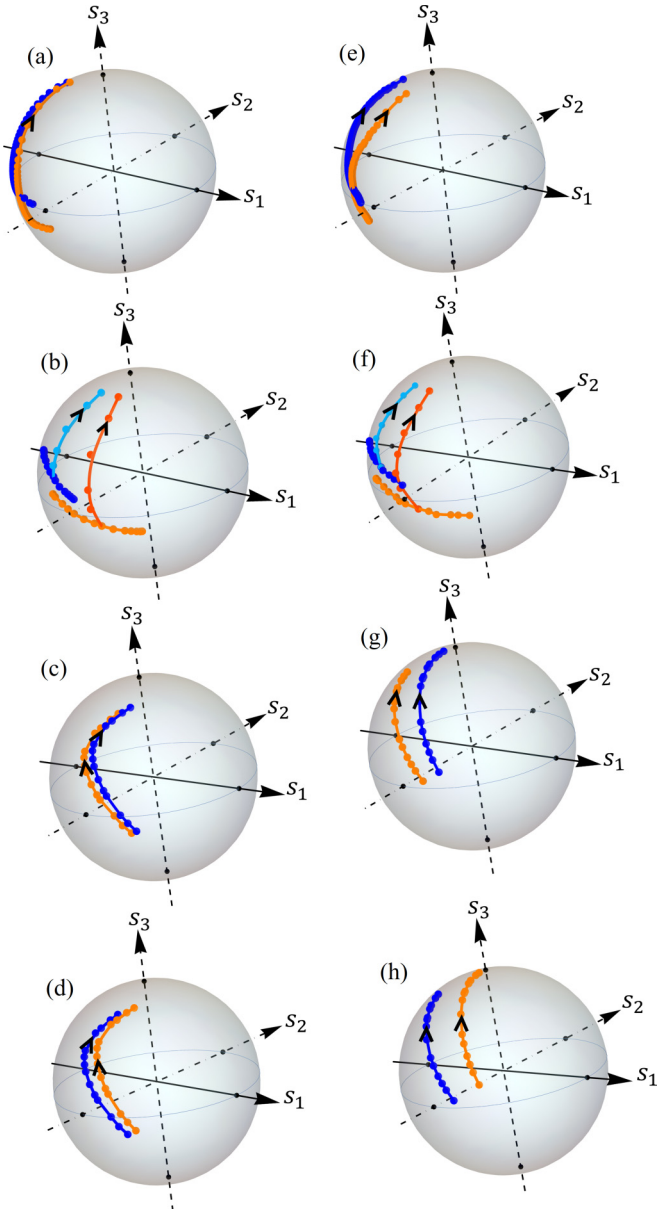


FIG. 6. Experimental and theoretical temperature dependence of the polarization of the $+2q_0$ (orange, light gray) and $-2q_0$ (blue, dark) diffraction peak for the LCP incident light for CB7CB (a–d) and CB6OCB (e–h). CB7CB: (a) experimental values, (b) preliminary model [48], (c) TMM, and (d) BPM. CB6OCB: (e) experimental values, (f) preliminary model [49], (g) TMM, and (h) BPM. The arrow heads represent the direction of temperature increase. Parameter values used in calculation are given in the text. The incident light is LCP.

diffraction peak. Due to the crudeness of the model the absolute values do not match, but it is obvious that BPM should be used for modeling, as expected, because the cell is thicker than the wavelength of light.

Next, we compared the experimental and theoretically predicted ratios of intensities between the zeroth ($I_0$), first ($I_1$), and second ($I_2$) order diffraction peaks (Fig. 7). The match is very good, considering the crudeness of the model. Also in the case of intensity ratios, the BPM is superior to TMM. By

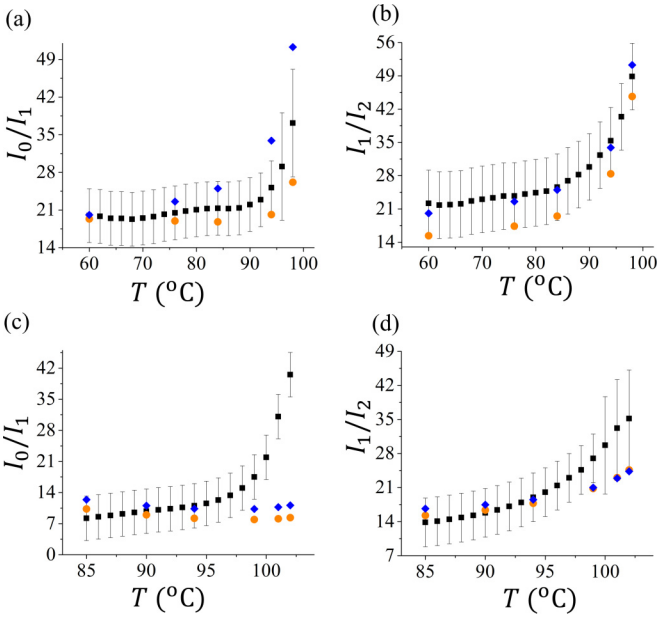


FIG. 7. Experimental and theoretically predicted ratios of intensities between the zeroth ($I_0$), first ($I_1$), and second ($I_2$) order diffraction peaks. (a), (b) CB7CB; (c), (d) CB6OCB. Black filled squares represent the experimental data and orange filled circles and blue filled diamonds show the theoretically calculated ratios from BPM and TMM, respectively.

repeating the calculations for the case of weak anchoring with a pretilt, we find that the polarization properties and ratios of intensities are best fitted for the strong anchoring condition, so we conclude that for these two materials the model with a pretilt of pseudolayers and strong anchoring describes best the experimental observations, especially for the CB7CB, for which there is also quantitative agreement.

The systematic discrepancies that we observe are in the azimuth angle of elliptical polarization of the second-order diffraction peaks, which is systematically too low. Also, the value of $q_{0s} - 1$ measured by the resonant soft x-ray scattering at the temperature of the stripe appearance is, by an order of magnitude, larger than the threshold value predicted by the model (see Table I). This could be due to the softening of the pseudolayer compressibility close to the phase transition. Indeed, as follows from Eq. (18), $q_{0s}^{(th)} \cong q_{0s}^{(\mathrm{expt})} \cong 1 + 10^{-2}$ if $\tilde{B} \cong 1 \times 10^3$ [59–61].

Finally, we would like to comment on the fact that for some materials (for example, material KA(0.2) in Ref. [45]) several intense diffraction peaks can be observed. This shows that the pseudolayer undulation is beyond the harmonic modulation and, probably, a sawtooth structure is formed [15,17].

Also, the intensity of the diffraction peaks strongly depends on the value of $\tilde{D}$. If it were exactly 2, one would observe only a weak first-order diffraction peak, because the form factor of one modulation period is zero for higher-order peaks. A small departure from 2 significantly increases intensities of higher-order diffraction peaks.

## IV. CONCLUSIONS

We have proposed a continuum model for the spontaneous formation of the stripe texture due to the 2D pseudolayer undulations in the thin cell with planar anchoring conditions filled with liquid crystalline material exhibiting the nematic to twist-bend nematic phase transition. Our study explains the effect of strong and weak boundary conditions on the threshold conditions for the pseudolayer undulations as well as the optical properties (intensity and polarization of the diffracted light) of the diffraction grating spontaneously formed in surface stabilized planar cells.

In the preliminary model [48,49], it was assumed that the angles $\alpha$ and $\beta$, defining the pseudolayer undulation, have the same amplitudes, but close to the phase transition temperature a faster reduction of $\beta$ was assumed ad hoc to account for the change of elliptical polarization of the second-order diffraction peak toward circularly polarized light. By the model presented in this paper we have shown that this difference in angles is inherent to the cell structure [see Eqs. (48) and (49); the difference is large especially close to the phase transition temperature, where $\tilde{D} < 2$]. Also, in the preliminary model the spatial variation of angles was slightly shifted to account for the asymmetry. By modeling the pseudolayer structure, the asymmetry enters the model due to the surface anchoring condition. If molecules are anchored in the surface plane, the helical cone axis will be tilted by the cone angle with respect to the surface. The model also gives a proper qualitative prediction of the polarization and intensity properties of the diffracted light.

## ACKNOWLEDGMENTS

This work was funded by the National Science Center (Poland) under Grant No. 2016/22/A/ST5/00319 and the Slovenian Research Agency (ARRS), through the Research Core Funding No. P1-0055. We thank Prof. C. T. Imrie for providing the compounds.

[1] Z. Chen, G. Huang, I. Trase, X. Han, and Y. Mei, Phys. Rev. Appl. **5**, 017001 (2016).
[2] T. Ishikawa and O. D. Lavrentovich, in *Defects and Undulation in Layered Liquid Crystals*, edited by O. D. Lavrentovich, P. Pasini, C. Zannoni, and S. Žumer, NATO Science Series (Series II: Mathematics, Physics and Chemistry), Vol. 43 (Springer, Dordrecht, 2001).
[3] H. Aharoni, D. V. Todorova, O. Albarran, L. Goehring, R. D. Kamien, and E. Katifori, Nat. Commun. **8**, 15809 (2017).
[4] L. E. Hough, H. T. Jung, D. Krüerke, M. S. Heberling, M. Nakata, C. D. Jones, D. Chen, D. R. Link, J. Zasadzinski, G. Heppke, J. P. Rabe, W. Stocker, E. Körblova, D. M. Walba, M. A. Glaser, and N. A. Clark, Science **325**, 456 (2009).
[5] W. Helfrich, Appl. Phys. Lett. **17**, 531 (1970).
[6] W. Helfrich, J. Chem. Phys. **55**, 839 (1971).
[7] J. P. Hurault, J. Chem. Phys. **59**, 2068 (1973).
[8] N. A. Clark and R. B. Meyer, Appl. Phys. Lett. **22**, 493 (1973).
[9] N. A. Clark and P. S. Pershan, Phys. Rev. Lett. **30**, 3 (1973).

[10] M. Delaye, R. Ribotta, and G. Durand, Phys. Lett. A **44**, 139 (1973).
[11] J. M. Delrieu, J. Chem. Phys. **60**, 1081 (1974).
[12] S. J. Singer, Phys. Rev. E **48**, 2796 (1993).
[13] J.-I. Fukuda and A. Onuki, J. Phys. II. **5**, 1107 (1995).
[14] I. W. Stewart, Phys. Rev. E **58**, 5926 (1998).
[15] S. J. Singer, Phys. Rev. E **62**, 3736 (2000).
[16] T. Ishikawa and O. D. Lavrentovich, Phys. Rev. E **63**, 030501(R) (2001).
[17] B. I. Senyuk, I. I. Smalyukh, and O. D. Lavrentovich, Phys. Rev. E **74**, 011712 (2006).
[18] G. Pelzl, A. Eremin, S. Diele, H. Kresse, and W. Weissflog, J. Mater. Chem. **12**, 2591 (2002).
[19] T. Niori, Y. Yamamoto, and H. Yokoyama, Mol. Cryst. Liq. Cryst. **409**, 475 (2004).
[20] W. Weissflog, S. Sokolowski, H. Dehne, B. Das, S. Grande, M. W. Schröder, A. Eremin, S. Diele, G. Pelzl, and H. Kresse, Liq. Cryst. **31**, 923 (2004).
[21] V. P. Panov, M. Nagaraj, J. K. Vij, Yu. P. Panarin, A. Kohlmeier, M. G. Tamba, R. A. Lewis, and G. H. Mehl, Phys. Rev. Lett. **105**, 167801 (2010).
[22] M. Cestari, S. Diez-Berart, D. A. Dunmur, A. Ferrarini, M. R. de la Fuente, D. J. B. Jackson, D. O. Lopez, G. R. Luckhurst, M. A. Perez-Jubindo, R. M. Richardson, J. Salud, B. A. Timimi, and H. Zimmermann, Phys. Rev. E **84**, 031704 (2011).
[23] R. B. Meyer, in *Molecular Fluids. Les Houches Lectures, 1973*, edited by R. Balian and G. Weill (Gordon and Breach, New York, 1976), p. 271.
[24] I. Dozov, Europhys. Lett. **56**, 247 (2001).
[25] R. Memmer, Liq. Cryst. **29**, 483 (2002).
[26] V. P. Panov, R. Balachandran, M. Nagaraj, J. K. Vij, M. G. Tamba, A. Kohlmeier, and G. H. Mehl, Appl. Phys. Lett. **99**, 261903 (2011).
[27] V. P. Panov, R. Balachandran, J. K. Vij, M. G. Tamba, A. Kohlmeier, and G. H. Mehl, Appl. Phys. Lett. **101**, 234106 (2012).
[28] D. Chen, J. H. Porada, J. B. Hooper, A. Klittnick, Y. Shen, M. R. Tuchband, E. Korblova, D. Bedrov, D. M. Walba, M. A. Glaser, J. E. Maclennan, and N. A. Clark, Proc. Natl. Acad. Sci. USA **110**, 15931 (2013).
[29] V. Borshch, Y. K. Kim, J. Xiang, M. Gao, A. Jákli, V. P. Panov, J. K. Vij, C. T. Imrie, M. G. Tamba, G. H. Mehl, and O. D. Lavrentovich, Nat. Commun. **4**, 2635 (2013).
[30] C. Meyer, G. R. Luckhurst, and I. Dozov, Phys. Rev. Lett. **111**, 067801 (2013).
[31] M. Salamończyk, N. Vaupotič, D. Pociecha, C. Wang, C. Zhu, and E. Gorecka, Soft Matter **13**, 6694 (2017).
[32] M. Salamończyk, R. J. Mandle, A. Makal, A. Liebman-Pelaez, J. Feng, J. W. Goodby, and C. Zhua, Soft Matter **14**, 9760 (2018).
[33] C. Meyer and I. Dozov, Soft Matter **12**, 574 (2016).
[34] I. Dozov and C. Meyer, Liq. Cryst. **44**, 4 (2017).
[35] M. P. Rosseto, L. R. Evangelista, P. S. Simonário, and R. S. Zola, Phys. Rev. E **101**, 012702 (2020).
[36] Z. Parsouzi, S. M. Shamid, V. Borshch, P. K. Challa, A. R. Baldwin, M. G. Tamba, C. Welch, G. H. Mehl, J. T. Gleeson, A. Jakli, O. D. Lavrentovich, D. W. Allender, J. V. Selinger, and S. Sprunt, Phys. Rev. X **6**, 021041 (2016).
[37] S. V. Shiyanovskii, P. S. Simonário, and E. G. Virga, Liq. Cryst. **44**, 31 (2017).
[38] S. M. Shamid, S. Dhakal, and J. V. Selinger, Phys. Rev. E **87**, 052503 (2013).
[39] N. Vaupotič, S. Curk, M. A. Osipov, M. Čopič, H. Takezoe, and E. Gorecka, Phys. Rev. E **93**, 022704 (2016).
[40] L. Longa and G. Pająk, Phys. Rev. E **93**, 040701(R) (2016).
[41] M. Čopič and A. Mertelj, Phys. Rev. E **101**, 022704 (2020).
[42] L. Longa and W. Tomczyk, J. Phys. Chem. C (2020), doi: 10.1021/acs.jpcc.0c05711.
[43] W. Tomczyk and L. Longa, Soft Matter **16**, 4350 (2020).
[44] V. P. Panov, J. K. Vij, R. Balachandran, V. Borshch, O. D. Lavrentovich, M. G. Tamba, and G. H. Mehl, Proc. SPIE **8828**, 88280X (2013).
[45] P. K. Challa, V. Borshch, O. Parri, C. T. Imrie, S. N. Sprunt, J. T. Gleeson, O. D. Lavrentovich, and A. Jakli, Phys. Rev. E **89**, 060501(R) (2014).
[46] V. P. Panov, M. C. M. Varney, I. I. Smalyukh, J. K. Vij, M. G. Tamba, and G. H. Mehl, Mol. Cryst. Liq. Cryst. **611**, 180 (2015).
[47] V. P. Panov, J. K. Vij, and G. H. Mehl, Liq. Cryst. **44**, 147 (2017).
[48] N. Vaupotič, M. Ali, P. W. Majewski, E. Gorecka, and D. Pociecha, Chem. Phys. Chem. **19**, 2566 (2018).
[49] M. Ali, N. Vaupotič, P. W. Majewski, E. Gorecka, C. Imrie, and D. Pociecha, Proc. SPIE. **10941**, 109410T (2019).
[50] R. C. Jones, J. Opt. Soc. Am. **31**, 488 (1941).
[51] G. L. Pedrola, *Beam Propagation Method for Design of Optical Waveguide Devices* (Wiley, Chichester, UK, 2016).
[52] E. Gorecka, N. Vaupotič, A. Zep, D. Pociecha, J. Yoshioka, J. Yamamoto, and H. Takezoe, Angew. Chem., Int. Ed. **54**, 10155 (2015).
[53] J. Chen and T. C. Lubensky, Phys. Rev. A **14**, 1202 (1976).
[54] S. Kralj and T. J. Sluckin, Phys. Rev. E **50**, 2940 (1994).
[55] N. Vaupotič, S. Kralj, M. Čopič, and T. J. Sluckin, Phys. Rev. E **54**, 3783 (1996).
[56] D. Pociecha, C. A. Crawford, D. A. Paterson, J. M. D. Storey, C. T. Imrie, N. Vaupotič, and E. Gorecka, Phys. Rev. E **98**, 052706 (2018).
[57] D. A. Paterson, M. Gao, Y. K. Kim, A. Jamali, K. L. Finley, B. R. Hernández, S. D. Berart, J. Salud, M. R. Fuente, B. A. Timimi, H. Zimmermann, C. Greco, A. Ferrarini, J. M. D. Storey, D. O. López, O. D. Lavrentovich, G. R. Luckhurst, and C.T. Imrie, Soft Matter **12**, 6827 (2016).
[58] M. R. Tuchband, D. A. Paterson, M. Salamończyk, V. A. Norman, A. N. Scarbrough, E. Forsyth, E. Garcia, C. Wang, J. M. D. Storey, D. M. Walba, S. Sprunt, A. Jákli, C. Zhu, C. T. Imrie, and N. A. Clark, Proc. Natl. Acad. Sci. USA **116**, 10698 (2019).
[59] S. M. Salili, C. Kim, S. Sprunt, J. T. Gleeson, O. Parri, and A. Jakli, RSC Adv. **4**, 57419 (2014).
[60] Z. Parsouzi, S. A. Pardaev, C. Welch, Z. Ahmed, G. H. Mehl, A. R. Baldwin, J. T. Gleeson, O. D. Lavrentovich, D. W. Allender, J. V. Selinger, A. Jaklic, and S. Sprunt, Phys. Chem. Chem. Phys. **18**, 31645 (2016).
[61] J. Zhou, W. Tang, Y. Arakawa, H. Tsuji, and S. Aya, Phys. Chem. Chem. Phys. **22**, 9593 (2020).